SUPPLEMENTARY INFORMATION

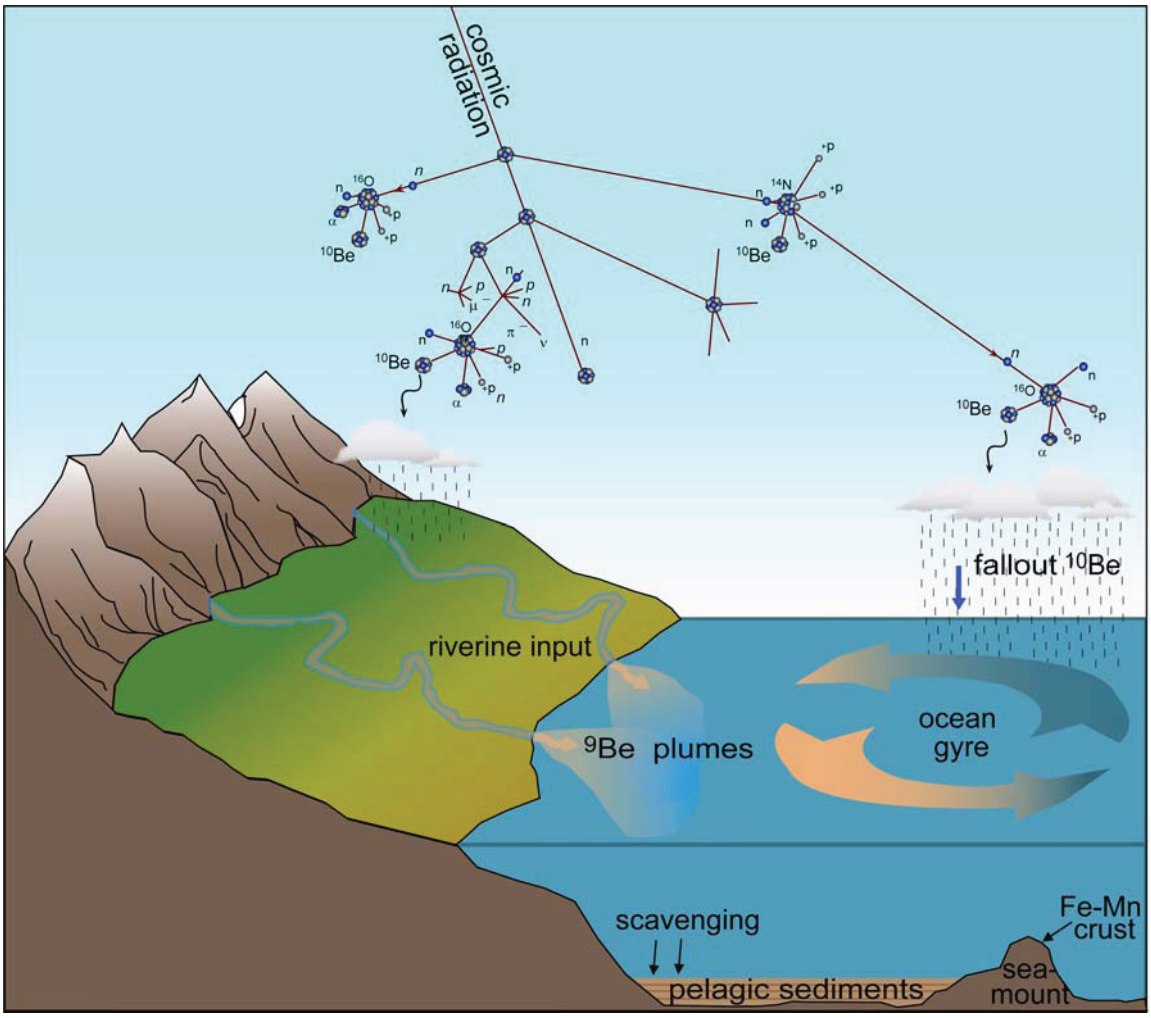

Schematic diagram showing how the $^{10}Be/^{9}Be$ ocean isotope proxy serves as tracer of global terrigenous input variations to the oceans. The constant-flux atmosphere-produced cosmogenic isotope ^{10}Be is mixed with the mostly riverine terrigenous stable isotope ^{9}Be when present in the dissolved form in the oceans. Both isotopes are scavenged at roughly equal rates into chemical deposits such as authigenic pelagic sediment and into hydrogenous ferromanganese crusts. There the isotope ratio is preserved back through time and, after correction for radioactive decay of ^{10}Be ($T_{1/2}$ = 1.39 My), can be used today to infer past variations of ^{9}Be input through changes in weathering and erosion. Figure A1 shows that this ratio was unchanged in the Atlantic, the Pacific, and the Arctic Ocean over the last ~12 My.

^{10}Be/^{9}Be ratios in Fe-Mn Crusts and Sediment Cores

Previously published Fe-Mn crusts and ocean core data that are presented in this manuscript have been modified from their original published state in a two ways that are described here and shown in Tables A1 and A2 and Figure A1.

First, the accepted value for the half-life of ^{10}Be has been modified from that used in the publications. There have been several determinations of the half-life of ^{10}Be in the past and most published ocean core and crust data were calculated using a half-life that is no longer widely supported. Values adopted by the cosmogenic community in the past have varied between 1.34 My and 1.51 My. Recently, a consensus was reached within the cosmogenic community that the half-life must be less than the previously widely used 1.51 My value (see Granger, 2006 and Nishiizumi et al. 2007 for details). Two new studies have reached a value of 1.387 My ± 0.012 My (Chmeleff et al., 2010; Korschinek et al., 2010) by independent techniques. Knowing and adapting to this lower half-life is important for calculating old (e.g. >1 My) Fe-Mn crusts and core ages and is crucial for restoring the ^{10}Be/^{9}Be ratio to its original value at the time of deposition to understand past ocean chemistry. We report the old and new values and thicknesses of crusts in Table A1 and ocean core depths sampled in Table A2. In cases in which both the growth rate of the crust or the sedimentation rate and the initial ^{10}Be/^{9}Be ratio is constant, the ^{10}Be/^{9}Be ratio versus crust thickness or core depth are best represented by a straight line in a log-normal plot (Fig A1a-c).

Using the ^{10}Be/^{9}Be ratio in Fe-Mn crusts or the authigenic phase in core sediment, the decay of ^{10}Be may be used for dating according to the following equation:

$$t = ln\ (R_t/R_o)/(-\lambda) \qquad \text{(Appendix-Eq. 1)}$$

where R_t is the measured ^{10}Be/^{9}Be ratio at time, t, R_o is the initial ratio at the time of sedimentation and λ is equal to ln(2)/half-life of the decaying nuclide (^{10}Be), which is 5.0×10^{-7} y^{-1} according to the new estimate (Chmeleff et al., 2009; Korschinek et al., 2009). The decrease of the measured authigenic phase ^{10}Be/^{9}Be ratio with depth of ocean core gives an estimate of the rate of sedimentation (Bourlès, 1988; Frank et al., 2008). Likewise, the decrease of the measured ^{10}Be/^{9}Be ratio with Fe-Mn crust thickness gives an estimate of the growth rate (Ku et al., 1982; von Blanckenburg et al., 1999). To determine the initial ratio of ^{10}Be/^{9}Be, we use the growth rate of the best fit-derived decay line to back-calculate the ratio at the time of Fe-Mn crust growth or sedimentation. Steady growth rates and the decay constant produce one unique solution. Sediment cores may be dated and their initial ^{10}Be/^{9}Be ratios can be determined in a similar way. Hiatuses in the sedimentary record are clearly disjointed series of measurements as seen in Frank et al. (2008).

Second, Bourlès et al. (1989) reports independently determined age estimates for the sediment in the core to restore the values to their initial ratio at the time of deposition. However, much progress has been made in the accepted magnetic timescale chronology since Bourlès et al. (1989) constructed their sedimentation curve. As noted in Granger (2006), the new timescale of Ogg and Smith (2004) should be used for this core. We calculate initial ratios with this new timescale and with the new ^{10}Be half-life of 1.39 My.

Third, further independent support is provided by the recently developed Os isotope stratigraphy for ferromanganese crusts CD29-2 and ALV-539 (Klemm et al., 2005; 2008), which agrees very well with the age information derived from ^{10}Be/^{9}Be for the past 10 Myr thus supporting the near constancy of the deepwater ^{10}Be/^{9}Be over the past 10 Myr.

Using both methods to calculate initial ratios, constant ^{10}Be/^{9}Be ratios result for the past 10 My. These ratios also agree with those measured today on surface scrapes of Fe-Mn crusts in the Atlantic and Pacific Oceans (Fig. A1d-A1e). In Arctic areas affected by sea ice, new biostratigraphic data and ^{10}Be/^{9}Be data on the adsorbed phase on sediment suggest that the ^{10}Be/^{9}Be ratio has increased within the past 0.5 My (Sellén et al., 2009).

Thus far, back-calculating the initial core sediment and Fe-Mn crust $^{10}Be/^{9}Be$ ratios at the time of deposition has relied on a number of assumptions concerning growth rate and how an increased flux of terrigenous ^{9}Be to the ocean would be manifested in the $^{10}Be/^{9}Be$ ratio. As a sensitivity test plotted in Figure A2, we modeled hypothetical curves showing the $^{10}Be/^{9}Be$ ratio versus crust depth for modeled 25% higher and lower crust growth rate for two Pacific Fe-Mn crusts that span the full range of growth rates for the dataset in Table A1. Fe-Mn crust data are not consistent with a 25% different modeled growth rate even for samples with high analytical uncertainties. New ages of the Fe-Mn crust data were calculated using the modeled 25% higher and lower growth rates in order to calculate the initial $^{10}Be/^{9}Be$ ratios from the time of deposition. These ages were then used to determine the modeled initial ratio assuming radioactive decay as in Fig A1d. We note that a 4-fold increase in apparent rates of terrigenous sediment accumulation in the ocean at 5 My (Hay et al., 1988) would be accompanied by a 4-fold increase in the flux of ^{9}Be. Even a 25% lower growth rate does not produce such a change in the modeled initial $^{10}Be/^{9}Be$ ratio.

We then modeled the core and Fe-Mn crust $^{10}Be/^{9}Be$ ratios versus crust depth for data and for changes in the ^{9}Be flux to the oceans. First , we assume that the ^{9}Be flux to the ocean increases as the flux of terrigenous sediment to the oceans increases and that both follow the apparent rates of terrigenous sediment accumulation in the oceans during the last 15 My according to Hay et al. (1988) (Fig. A3a). We also keep the modern $^{10}Be/^{9}Be$ ratio at its present value. The resulting curve shows that terrestrial material flux into the oceans of Hay et al. (1988) is not reflected in the $^{10}Be/^{9}Be$ ratios. This disparity between modeled expectation and data may be because either the apparent terrestrial fluxes were not real terrestrial fluxes, as described in the main text or that there was some compensating factor. In order to increase the ^{9}Be and maintain the constant ^{9}Be observations, a decrease in crust growth rate is required. A decrease in the Fe-Mn crust growth rate could balance increased ^{9}Be fluxes. However, with increased ^{9}Be and presumably coeval increases in other metal concentrations in the ocean, we would expect that Fe-Mn crusts would instead have an increased growth rate. Moreover, the RC65-12 core with independent chronology from magnetostratigraphy does not show this required increase in sedimentation rate in the recent part of the record. In fact, the sedimentation rate in this core decreases toward the present. We also model the effect of abrupt increases in ^{9}Be with magnitude of terrigenous flux through time from Hay et al. (1988). Such an abrupt increase produces a discontinuity in the curve which is not apparent in the crust or core data.

Meteoric ^{10}Be and ^{9}Be input through Dust

The flux of dust to oceans potentially provides an additional component to the $^{10}Be/^{9}Be$ ratio through time. von Blanckenburg et al. (1996) provided an initial assessment of the potential of changes in the effect of dust on the $^{10}Be/^{9}Be$ ratio and found that ^{9}Be originating from dust does not explain the large fluxes of ^{9}Be to the oceans. Although the interpretation given in von Blanckenburg et al. (1996) is correct, the calculations provided in this study did not take into account the contribution of ^{10}Be on the dust particles as well. Adding this component of the dust decreases the potential of dust as a major source of ^{9}Be. Based on a modification of the analysis of von Blanckenburg et al. (1996) to include both ^{10}Be and ^{9}Be fluxes to the ocean, Figure A4 shows the potential contribution of dust to the $^{10}Be/^{9}Be$ ratio. Note that unrealistically high degrees of dissolution are still required to balance the ocean ^{9}Be budget, suggesting that another ^{9}Be source is required. Adding ^{10}Be to the analysis strengthens the original argument.

If rates of dust dissolution in the oceans are ~10% (Brown et al., 1992) and average concentration of ^{9}Be in dust is ~2.3 ppm (Chester, 1990), then the annual global dust flux of ~10^{3} mg m^{-2} y^{-1} (Jickells et al., 2005) mostly intercepts the possible dissolution rates between 1 and 2 orders of magnitude above the observed $^{10}Be/^{9}Be$ ratio. These relationships are plotted in Fig. A4 for various degrees of dust dissolution. Even if the ocean chemistry was such that all dust was completely dissolved on entering the ocean (100% dissolution line), dissolution rates for terrigenous matter would likely also be higher than normal. Variable concentrations of ^{10}Be on dust range from a maximum of 10^{10} atom g^{-1} (Baumgartner et al., 1997) to a possible minimum of 10^{7} atom g^{-1} (Sugden et al., 2009; Willenbring and von Blanckenburg, 2010). Assuming 10% dissolution of clay minerals (Brown et al., 1992), the

flux only reaches the expected $^{10}Be/^{9}Be$ ratio of $1x10^{-7}$ within the center of a dust plume when the dust fluxes are 10^4 mg m^{-2} y^{-1}. However, our database of cores and crusts have locations that span areas of known dust plumes. Yet, all cores show similar behavior over time, indicating that if dust flux is a factor in contributing ^{9}Be in some areas and if erosion rates had changed over these intervals, a change in the dust flux or terrigenous erosion would have had opposite magnitudes. Core and crust locations are also in nearly open water which should give a globally averaged flux of ^{9}Be to the ocean and minimize effects of specific geologically active regions contributing to a local signal (Igel and von Blanckenburg, 1999, von Blanckenburg and Igel, 1999).

Paleo CO_2 proxies

Figure A5 shows the raw data used for the shaded bands that span pCO_2 estimates and their uncertainties shown in the main text, Figure 1. Data points are from ocean proxies (Royer et al., 2004) and stromatal indices (Royer et al., 2004; Kürschner et al., 2008). Recent alkenone estimates are those cited in (Pagani et al., 2010) encompassing the pCO_2 data and uncertainties.

Appendix References

Baumgartner, S., Beer, J., Wagner, G., Kubik, P.W., Suter, M., Raisbeck, G.M., Yiou, F. 1021 1997. ^{10}Be and dust. Nuclear Instruments and Methods B123: 296-301.

Bourlès, D., Raisbeck, G.M., Yiou, F. 1989. ^{10}Be and ^{9}Be in marine sediments and their potential for dating. Geochimica et Cosmochima Acta 5: 443-452.

Bourlès, D. 1988. Etude de la geochimie de l'isotope cosmogenique ^{10}Be et de son isotope stable ^{9}Be en milieu oceanique. Application la datation des sediments marins. Ph.D. thesis, Univ. Paris XI.

Brown E.T., Measures C.I., Edmond J.M., Bourlès D.L., Raisbeck G.M., Yiou F. 1992. Continental inputs of beryllium to the oceans. Earth and Planetary Science Letters 114:101-111

Chester, R. 1990. Marine Geochemistry, Unwin Hyman, London, 698 pp.

Chmeleff J., von Blanckenburg F., Kossert K., Jacob D., 2010. Determination of the ^{10}Be half-life by multicollector ICP-MS and liquid scintillation counting. Nuclear Instruments and Methods B 268: 192-199.

Frank, M., Backman, J., Jakobsson, M., Moran, K., O'Regan, M., King, J., Haley, B.A., Kubik, P.W. Garbe-Schönberg, D. 2008. Beryllium isotopes in central Arctic Ocean sediments over the past 12.3 million years: Stratigraphic and paleoclimatic implications. Paleoceanography 23, PA1S02, doi:10.1029/2007PA001478.

Granger, D. 2006. A review of burial dating methods using ^{26}Al and ^{10}Be. Geological Society of America, special paper 415, Edited by Lionel L. Siame, Didier L. Bourlès, and Erik T. Brown: 1-16.

Hay, W.W., Sloan, J.L.I., and Wold, C.N. 1988. The mass/age distribution of sediments on the ocean floor and the global rate of loss of sediment. Journal of Geophysical Research 93: 14933-14940.

Igel, H., von Blanckenburg, F. 1999. Lateral mixing and advection of reactive isotope tracers in ocean basins: numerical modeling. Geochemistry, Geophysics, Geosystems 1:1999GC000003.

Jickells,T.D., An,Z.S., Andersen, K.K., Baker, A.R., Bergametti, G., Brooks, N., Cao, J.J., Boyd, P.W., Duce, R.A., Hunter, K.A., Kawahata, H., Kubilay, N., laRoche, J., Liss, P.S., Mahowald, N., Prospero, J.M., Ridgwell, A.J., Tegen, I., Torres, R. 2005. Global Iron Connections between Desert Dust, Ocean Biogeochemistry, and Climate. Science 308: 67-70. DOI: 10.1126/science.1105959.

Klemm, V., Levasseur, S., Frank, M., Hein, J.R., and Halliday, A.N. 2005. Osmium isotope stratigraphy of a marine ferromanganese crust. Earth and Planetary Science Letters 238, 42-48.

Klemm, V., Frank, M., Levasseur, S., Halliday, A.N., and Hein, J.R. 2008. Seawater osmium isotope evidence for a middle Miocene flood basalt event in ferromanganese crust records. Earth and Planetary Science Letters 273, 175-183.

Korschinek, G., Bergmaier, A., Faestermann, T., Gerstmann, U.C., Knie, K., Rugel, G., Wallner, A., Dillmann, I., Dollinger, G., Lierse von Gostomskie, C., Kossert, K., Maitia, M., Poutivtsev, M., Remmert, A. 2010. A new value for the half-life of ^{10}Be by heavy ion elastic recoil detection and liquid scintillation counting Nuclear Instruments and Methods B 268: 187-191.

Ku, T.L., Kuskabe, M., Nelson, D.E., Southon, J.R., Korteling, R.G., Vogel, J., Nowikow, I. 1982. Constancy of Oceanic Deposition of ^{10}Be as recorded in Manganese Crusts. Nature 299: 240-242.

Kürschner, W.M., Kvakčec, Z., Dilcher, D.L. 2008. The impact of Miocene atmospheric carbon dioxide fluctuations and the evolution of terrestrial ecosystems. Proceedings of the National Academy of Sciences 105: 449–453.

Ling, H.F., Burton, K.W., O'Nions, R.K., Kamber, B., von Blanckenburg, F., Gibb, A.J., Hein, J.R., 1997. Evolution of Nd and Pb isotopes in Central Pacific seawater from ferromanganese crusts. Earth and Planetary Science Letters 146: 1–12.

Lüthi, D., Le Floch, M., Bereiter, B., Blunier, T., Barnola, J.-M, Siegenthaler, U., Raynaud, D., Jouzel, J., Fischer, H.,Kenji Kawamura, K., Stocker, T.F. 2007. High-resolution carbon dioxide concentration record 650,000–800,000 years before present. Nature Geoscience 453: 379-382.

Middleton, R., Brown, L., Dezfouly-Arjomandy, B., Klein, J. 1993. On ^{10}Be standards and the half-life of ^{10}Be: Nuclear Instruments and Methods in Physics Research B82: 399-403.

Nishiizumi K., Imamura M., Caffee M.W., Southon J.R., Finkel R.C., McAninch J. 2007. Absolute calibration of Be-10 AMS standards. Nuclear Instruments and Methods in Physics Research B 25 403-413.

Ogg J.G., Smith A.G. 2004. The Geomagnetic Polarity Time Scale. In: Gradstein F.M., Ogg J.G., & Smith A.G. (eds.), A Geological Time Scale, Cambridge University Press, Cambridge, 63-95.

O'Nions R.K., Frank M., von Blanckenburg F., Ling H.F. 1998. Secular variations of Nd and Pb isotopes in ferromanganese crusts from the Atlantic, Indian, and Pacific Oceans. Earth and Planetary Science Letters 155:15-28

Pagani, M., Liu, Z. LaRiviere, J., Ravelo, C., 2010. High Earth-system climate sensitivity determined from Pliocene carbon dioxide concentrations. Nature Geoscience 3: 27 - 30. doi:10.1038/ngeo724.

Royer, D.L., Berner, R.A., Montañez, I.P., Tabor, N.J., & Beerling, D.J. 2004. CO_2 as a primary driver of Phanerozoic climate change. GSA Today 14: 4-10.

Segl, M., Mangini, A., Bonari, G., Suter, M., Wolfi, W. 1989. Growth rate variations of manganese nodules and crusts induced by paleoceanographic events. Paleoceanography 4: 511-530.

Sellén, E., Jakobsson, M., Frank, M., Kubik, P.W. 2009. Pleistocene variations of beryllium isotopes in central Arctic Ocean sediment cores. Global and Planetary Change 68: 38-47.

Sugden, D.E. McCulloch, R.D., Bory, A.J.-M., Hein, A.S. 2009. Influence of Patagonian glaciers on Antarctic dust deposition during the last glacial period. Nature Geoscience 2: 281 – 285.

van de Flierdt, T., Frank, M., Halliday, A.N., Hein, J.R., Hattendorf, B., Gunther, D., and Kubik, P.W., 2004, Deep and bottom water export from the Southern Ocean to the Pacific Ocean over the past 38 million years. Paleoceanography 19, PA 1020, 10.1029/2003PA000923.

von Blanckenburg, F., Igel, H. 1999. Lateral mixing and advection of reactive isotope tracers in ocean basins: observations and mechanisms. Earth and Planetary Science Letters 169: 113-128.

von Blanckenburg, F., O'Nions, R.K., Belshaw, N.S., Gibb, A., Hein, J.R. 1996. Global distribution of Beryllium isotopes in deep ocean water as derived from Fe-Mn crusts. Earth and Planetary Science Letters 141: 213-226.

von Blanckenburg, F., O'Nions, R. K. 1999. Response of beryllium and radiogenic isotope ratios in Northern Atlantic Deep Water to the onset of northern hemisphere glaciation. Earth and Planetary Science Letters 167(3-4): 175-182.

Willenbring, J.K. and von Blanckenburg, F. 2010. Meteoric cosmogenic Beryllium-10 adsorbed to river sediment and soil: applications for Earth-surface dynamics. Earth Science Reviews 98: 105–122. doi:10.1016/j.earscirev.2009.10.008.

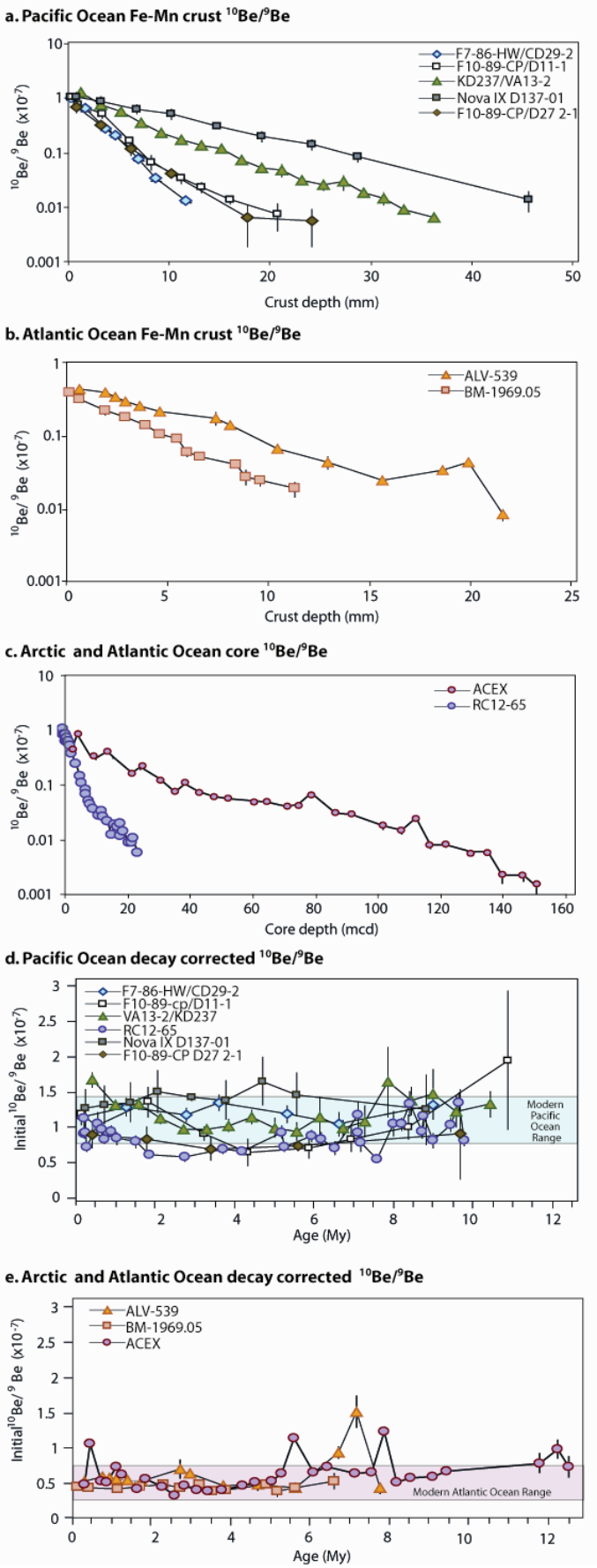

Figure A1: $^{10}Be/^{9}Be$ ratio versus crust depth in the **a.)** Pacific Ocean; **b.)** Atlantic Ocean; **c.)** ocean cores in the Pacific and Arctic. Data are from sources described in Table A1 and A2. After assuming constant growth rates for ferromanganese crusts and steady and intermittent sedimentation rates in ocean cores, the initial ratios in oceans at the time of deposition can be corrected for radioactive decay. **d.)** Pacific ocean ratios and analytical uncertainty are plotted versus the calculated age. Where error bars are not shown, the uncertainty lies within the size of the plotted point. In the case of the core RC12-65, the initial ratios were calculated based on paleomagnetic ages. However, using the steady sedimentation rates method yields similar time-corrected results. **e.)** Arctic and Atlantic Ocean ratios and analytical uncertainty are plotted versus the calculated time. Age uncertainties are not propagated into decay-corrected ratios in Fig. d and e, but the effect of such error is investigated in Fig. A2.

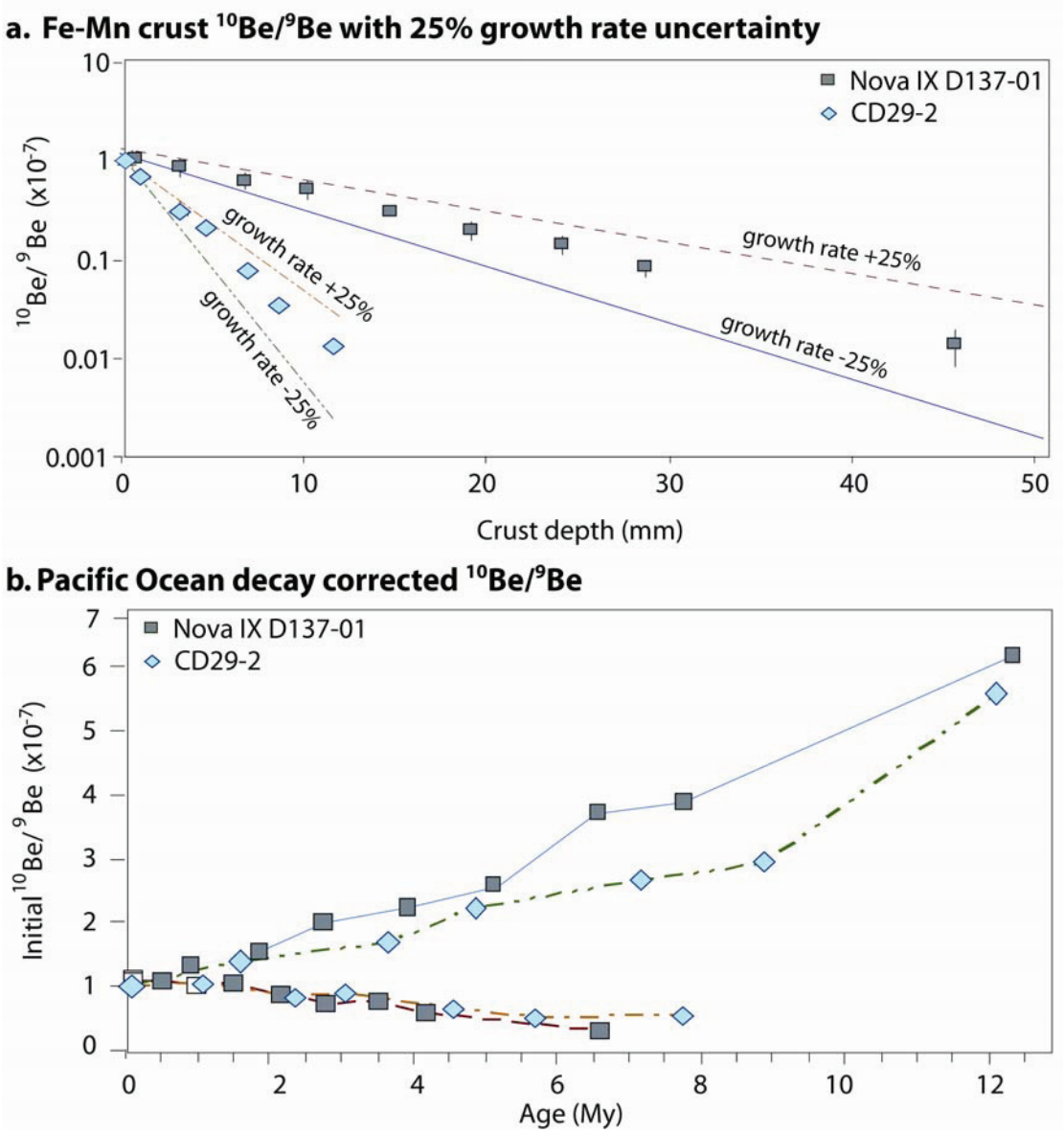

Figure A2. a.) Fe-Mn crust $^{10}Be/^{9}Be$ ratios versus crust depth and for modeled 25% higher and lower crust growth rate. Modeled lines and data are shown for the highest growth rate of the crusts in Table A1 (Nova IX D137-01) and the crust with the lowest growth rate (CD29-2) in Table A1. Note that the data including their analytical uncertainties are not consistent with a 25% different modeled growth rate. **b.)** As a sensitivity test, new decay-corrected $^{10}Be/^{9}Be$ ratios of the Fe-Mn crust data were calculated using the modeled 25% higher (red and orange) and lower (blue and green) growth rates. We note that a 4-fold increase in apparent rates of terrigenous sediment accumulation in the ocean at 5 My (Hay et al., 1988) should be accompanied by a 4-fold increase in the flux of ^{9}Be. Even a 25% lower growth rate does not produce such a change in the $^{10}Be/^{9}Be$ ratio of this magnitude.

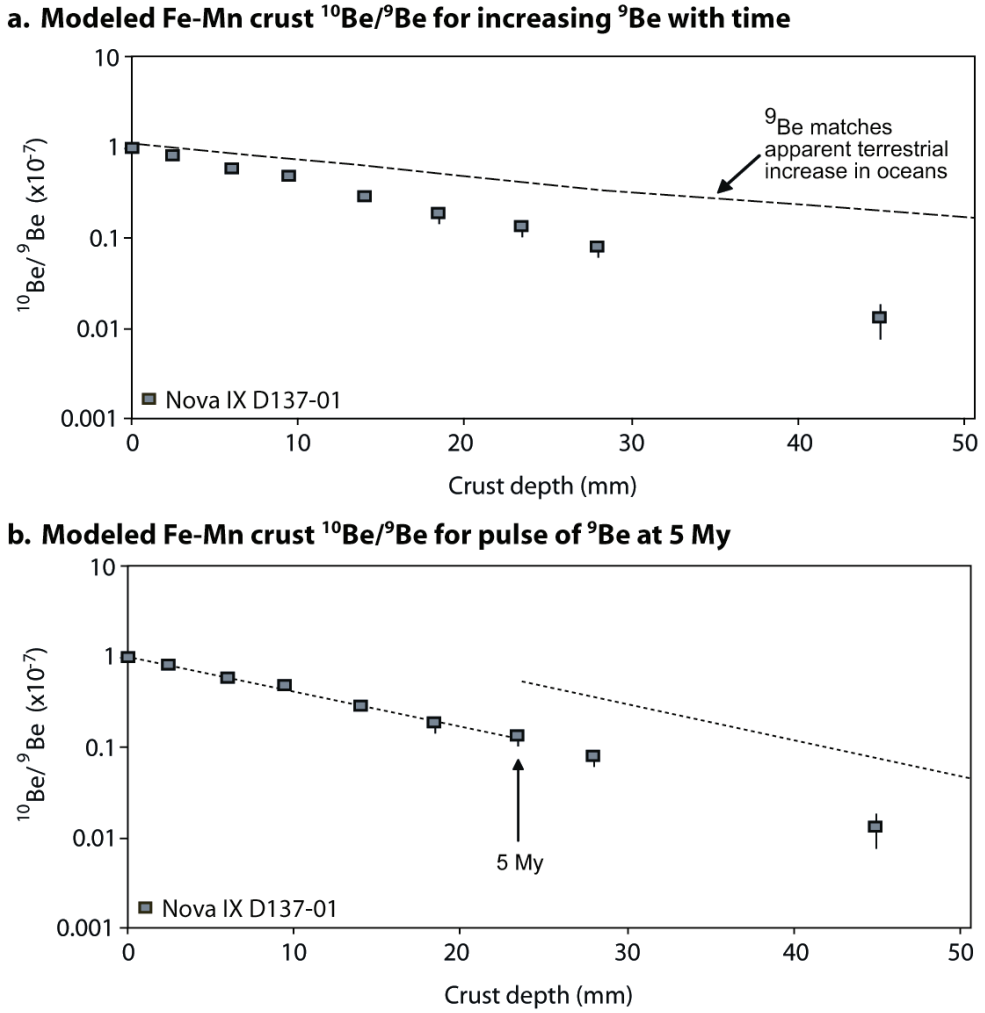

Figure A3. Fe-Mn crust $^{10}Be/^{9}Be$ ratios versus crust depth for data and for modeled changes in the ^{9}Be flux to the oceans. **a.)** The dashed line plotted here assumes that the ^{9}Be into a Fe-Mn crust increases proportionally to the constant ^{10}Be flux as the flux of terrigenous sediment to the oceans increases and that both follow the apparent rates of terrigenous sediment accumulation in the oceans during the last 15 My according to Hay et al. (1988). **b.)** The dashed line plotted here assumes that there was an abrupt increase (4-fold) in the flux of ^{9}Be to the oceans at 5 My. Such an abrupt increase is not apparent in the crust or core data.

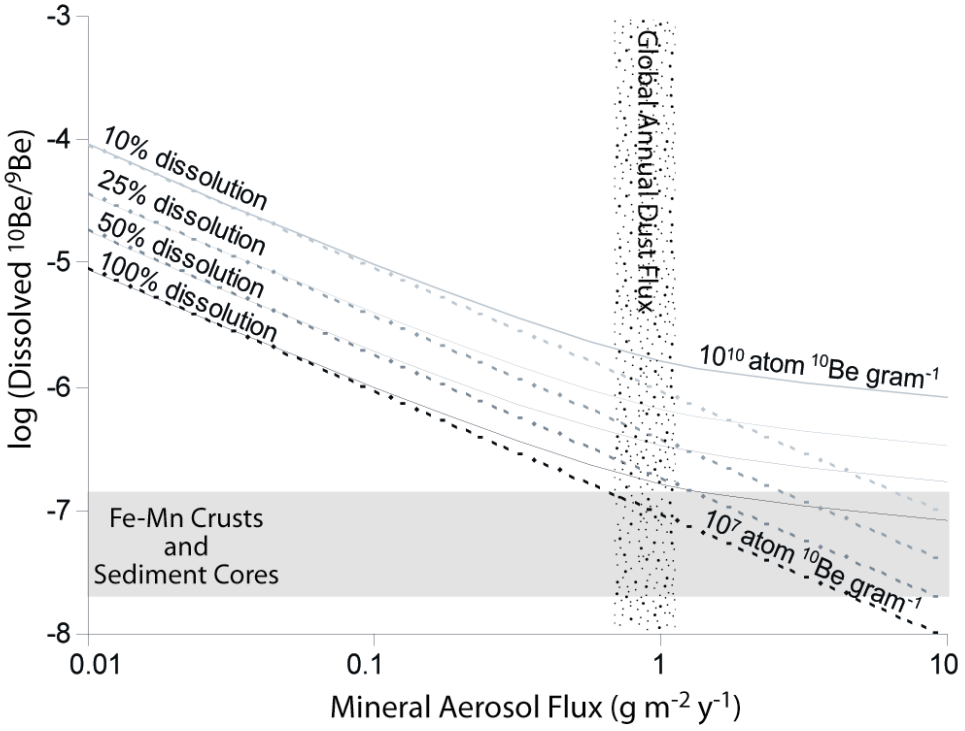

Figure A4. The modelled contribution of dust possibly contained within the ocean ratio of ^{10}Be/^{9}Be. This analysis was modified from that of von Blanckenburg et al (1996) by adding meteoric ^{10}Be adsorbed to dust particles. Variable concentrations of ^{10}Be on dust of 10^{10} atom g^{-1} (solid lines) and 10^{7} atom g^{-1} (dashed lines) represent the maximum reported concentrations (Baumgartner et al., 1997) and the low concentrations typical of areas with high erosion rates that could contribute large quantities of dust (Sugden et al., 2009; Willenbring and von Blanckenburg, 2010). While desorption of meteoric ^{10}Be was assumed to be 100% throughout, the fraction of ^{9}Be entering seawater in the dissolved form was approximated by using various degrees of dust dissolution. Reported rates of dust dissolution in the oceans are ~10% (Brown et al., 1992) and average concentration of ^{9}Be in dust is ~2.3 ppm (Chester, 1990). Ferromanganese crusts show a ratio that only intersects the global dust flux line at an unrealistic value of 100% dissolution. The above analysis shows that the annual global dust flux of ~1 g m^{-2} y^{-1} (stippled bar: Jickells et al., 2005) mostly intercepts the possible dissolution rates (gray and black lines) between 1 and 2 orders of magnitude above the observed ^{10}Be/^{9}Be ratio. Even if the ocean chemistry was such that all dust was completely dissolved on entering the ocean, dissolution rates for terrigenous matter would likely also be higher than normal.

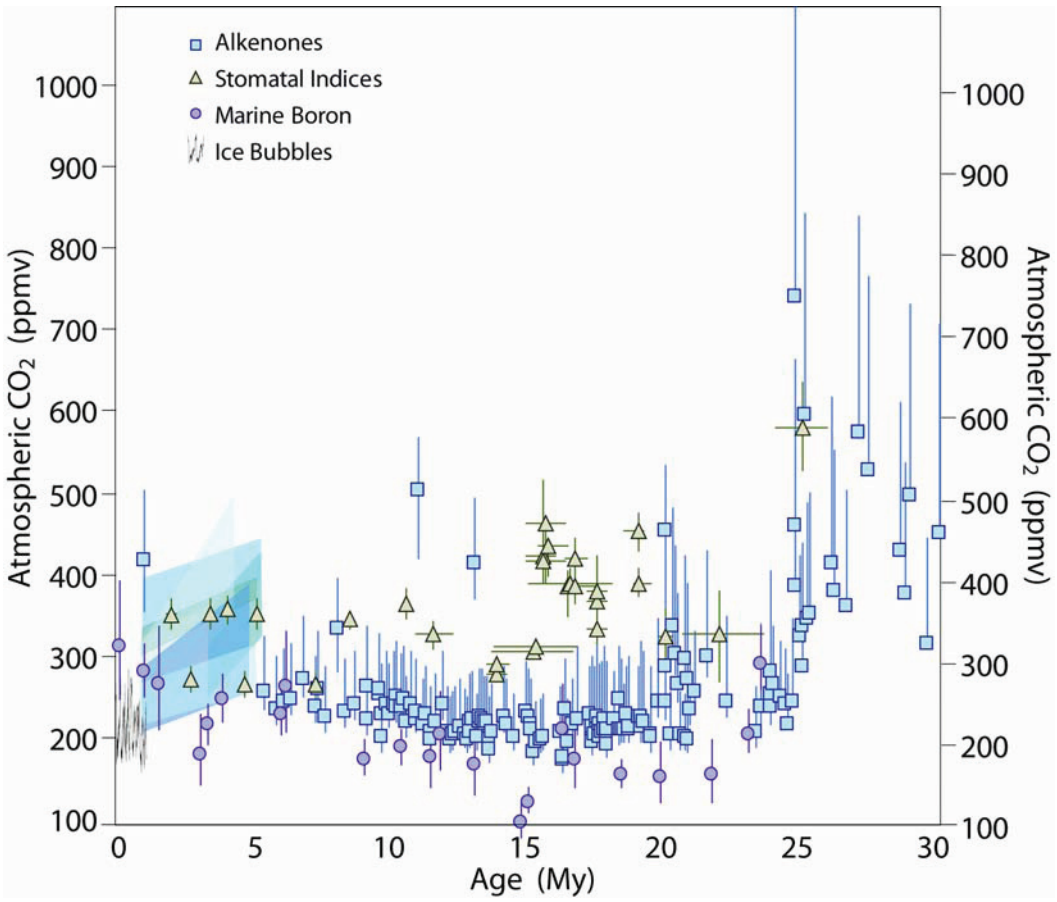

Figure A5. Late Cenozoic atmospheric CO_2. The CO_2 data include those data cited in the compilation in Royer et al. (2004) and are derived from a number of independent proxies. These show approximately steady atmospheric concentrations from mid-Miocene to pre-industrial values. Proxies in the Royer et al. (2004) compilation include: boron isotopes in planktonic foraminifera (purple circles), stomatal distribution in the leaves of C_3 plants (green triangles), the $\delta^{13}C$ of alkenones (blue squares). More recent data that are not cited in the Royer et al. (2004) compilation are included in this figure such as those Pliocene $\delta^{13}C$ of alkenones represented as blue bands spanning data ranges given in Pagani et al. (2010). In addition, the figure shows mid-Miocene CO_2 estimates from stromatal distribution in leaves from Kürschner et al. (2008). Data cited in Lüthi et al. (2007) shown in the figure with a thin black line extends the Antarctic ice bubble record to ~800 ky up to recent time.

Table A1. Fe-Mn crust $^{10}Be/^{9}Be$ ratios, depth, and ages

Crust	Reference	Depth mm	$^{10}Be/^{9}Be$ measured $x10^{-7}$	$^{10}Be/^{9}Be$ Error $x10^{-7}$	Age from Decay Calculation My	Mean Growth Rate mm/My	Age from Growth Rate My	Time-corrected $^{10}Be/^{9}Be_{init}$ $x10^{-7}$	Time-corrected Error $x10^{-7}$
F7-86-HW/CD29-2 (Pacific)	*von Blanckenburg et al., 1996*	0.0	1.1200	0.112	0.00		0.00	1.120	0.112
		1.5	0.7100	0.071	1.30	1.24	1.17	1.277	0.128
		3.4	0.3000	0.025	3.02		2.75	1.187	0.097
	Ling et al., 1997	4.5	0.2280	0.019	3.57		3.60	1.380	0.116
		6.7	0.0844	0.009	5.56		5.38	1.244	0.127
		8.4	0.0381	0.006	7.15		6.76	1.118	0.179
		11.4	0.0145	0.002	9.08		9.23	1.461	0.155
F10-89-CP/D11-1 (Pacific)	*von Blanckenburg et al., 1996*	0.0	1.1600	0.090	0.00		0.00	1.177	0.091
		0.7	0.8250	0.068	0.68	1.88	0.37	0.994	0.082
		3.2	0.5700	0.090	1.42		1.70	1.334	0.211
		5.9	0.1840	0.020	3.68		3.13	0.882	0.096
	Ling et al., 1997	8.0	0.0748	0.022	5.48		4.25	0.626	0.184
		11.0	0.0369	0.007	6.90		5.82	0.676	0.128
		13.0	0.0258	0.005	7.61		6.91	0.815	0.171
		15.8	0.0149	0.003	8.71		8.37	0.977	0.171
		20.5	0.0083	0.004	9.89		10.89	1.914	0.973
KD237/VA13-2 (Pacific)	*Segl et al., 1989*	1	1.4200	0.086	0.00		0.29	1.642	0.099
		3	0.8300	0.028	1.07	3.44	0.87	1.283	0.044
		5	0.6300	0.036	1.63		1.45	1.302	0.075
		7	0.3980	0.025	2.54		2.03	1.100	0.070
		9	0.2580	0.014	3.41		2.61	0.953	0.051
		11	0.1920	0.010	4.00		3.19	0.948	0.051
		13	0.1510	0.013	4.48		3.77	0.997	0.086
		15	0.1270	0.010	4.83		4.36	1.121	0.092
		17	0.0820	0.011	5.70		4.94	0.967	0.131
		19	0.0580	0.008	6.40		5.52	0.915	0.125
		21	0.0530	0.013	6.58		6.10	1.117	0.275
		23	0.0340	0.004	7.46		6.68	0.958	0.116
		25	0.0280	0.006	7.85		7.26	1.055	0.219
		27	0.0320	0.010	7.59		7.84	1.612	0.492
		29	0.0200	0.003	8.53		8.42	1.347	0.193
		31	0.0160	0.004	8.97		9.00	1.441	0.351
		33	0.0100	0.002	9.91		9.58	1.204	0.226
		36	0.0070	0.001	10.63		10.45	1.302	0.180
Nova/ IX D137-01	*van de Flierdt et al., 2004*	0.5	1.1880	0.243	0.27		0.10	1.247	0.255
		3	0.9670	0.199	0.68	5.17	0.58	1.293	0.266
		6.5	0.7050	0.145	1.31		1.26	1.322	0.272
		10	0.5610	0.114	1.77		1.94	1.476	0.300
		14.5	0.3440	0.012	2.75		2.81	1.399	0.049
		19	0.2160	0.044	3.68		3.68	1.358	0.277
		24	0.1590	0.033	4.29		4.64	1.621	0.336
		28.5	0.0910	0.019	5.41		5.51	1.434	0.299
		45.5	0.0150	0.006	9.01		8.80	1.224	0.490
F10-89/CP D27	*van de Flierdt et al., 2004*	0.5	0.7620	0.162	0.05		0.28	0.875	0.186
		3	0.3550	0.074	1.57	1.81	1.66	0.813	0.169
		6	0.1280	0.031	3.61		3.31	0.671	0.163
		10	0.0450	0.001	5.71		5.52	0.713	0.016
		17.5	0.0070	0.005	9.43		9.67	0.880	0.628
		24	0.0060	0.004	9.74		13.26	4.541	3.027

ALV-539 (Atlantic)	*von Blanckenburg et al., 1996*	0.5	0.4330	0.026	0.00		0.18	0.473	0.028
		1.8	0.3880	0.014	0.22	2.83	0.64	0.533	0.019
		2.3	0.3460	0.014	0.45		0.81	0.520	0.021
		2.8	0.2990	0.016	0.74		0.99	0.491	0.026
		3.5	0.2580	0.009	1.04		1.24	0.479	0.016
		4.5	0.2130	0.012	1.42		1.59	0.472	0.027
	von Blanckenburg and O'Nions. 1999	7.3	0.1740	0.034	1.82		2.58	0.633	0.124
		8	0.1400	0.008	2.26		2.83	0.576	0.035
		10.3	0.0659	0.006	3.77		3.64	0.407	0.035
		12.8	0.0436	0.008	4.59		4.53	0.419	0.081
		15.5	0.0242	0.002	5.77		5.48	0.375	0.031
		18.5	0.0330	0.003	5.15		6.54	0.870	0.078
		19.8	0.0436	0.006	4.59		7.00	1.447	0.212
		21.5	0.0082	0.001	7.94		7.61	0.367	0.066
BM-1969.05 (Atlantic)	*von Blanckenburg et al., 1996*	0	0.3940	0.032	0.00		0.00	0.394	0.032
	von Blanckenburg and O'Nions. 1999; O'Nions et al., 1998	0.5	0.3230	0.012	0.40	1.74	0.29	0.373	0.014
		1.75	0.2190	0.025	1.17		1.01	0.362	0.041
		2.75	0.1796	0.008	1.57		1.58	0.396	0.018
		3.75	0.1410	0.006	2.06		2.16	0.414	0.018
		4.5	0.1040	0.007	2.66		2.59	0.379	0.026
		5.35	0.0899	0.005	2.96		3.08	0.418	0.024
		5.85	0.0598	0.009	3.77		3.36	0.321	0.047
		6.5	0.0520	0.004	4.05		3.74	0.337	0.029
		8.25	0.0394	0.003	4.61		4.74	0.422	0.028
		8.75	0.0269	0.006	5.37		5.03	0.333	0.077
		9.5	0.0239	0.004	5.60		5.46	0.367	0.061
		11.2	0.0185	0.004	6.12		6.44	0.463	0.110

Table A2. Sediment core $^{10}Be/^{9}Be$ ratio, depth, ages

Core	Reference	Depth	$^{10}Be/^{9}Be$ measured	$^{10}Be/^{9}Be$ Error	Age Calc from Decay	Mean Growth Rate	Age from Growth Rate	Time-corrected $^{10}Be/^{9}Be_{init}$	Time-corrected Error	Independent Chronology
		mcd	x10^{-7}	x10^{-7}	My	m/My	My	x10^{-7}	x10^{-7}	My
RC12-65 (Pacific)	*Bourlès et al., 1989*	0.120	0.8580	0.0620	0.00		0.09	0.883	0.064	0.057
		0.190	1.0630	0.0820	-0.43	1.38	0.14	1.101	0.085	0.070
		0.310	0.8570	0.0750	0.00		0.22	0.897	0.078	0.091
		0.890	0.6460	0.0560	0.57		0.64	0.696	0.060	0.149
		1.100	0.8350	0.1200	0.05		0.80	1.033	0.149	0.426
		1.210	0.7240	0.0920	0.34		0.88	0.942	0.120	0.527
		1.580	0.6100	0.0530	0.68		1.14	0.815	0.071	0.580
		1.740	0.6250	0.0550	0.63		1.26	0.913	0.080	0.757
		2.250	0.5270	0.0540	0.97		1.63	0.822	0.084	0.889
		2.625	0.3860	0.0450	1.60		1.90	0.772	0.090	1.387
		3.925	0.2470	0.0220	2.49		2.84	0.594	0.053	1.754
		5.300	0.1480	0.0140	3.51		3.83	0.557	0.053	2.652
		6.100	0.1080	0.0100	4.14		4.41	0.662	0.061	3.626
		7.350	0.0825	0.0076	4.68		5.32	0.644	0.059	4.109
		7.430	0.0700	0.0064	5.01		5.38	0.908	0.083	5.126
		8.250	0.0521	0.0049	5.60		5.97	0.699	0.066	5.193
		8.650	0.0450	0.0041	5.90		6.26	0.852	0.078	5.882
		9.450	0.0374	0.0041	6.27		6.84	0.808	0.089	6.145
		11.250	0.0272	0.0037	6.90	3.65	6.96	0.688	0.094	6.461
		12.275	0.0337	0.0053	6.47		7.24	1.155	0.182	7.069
		12.625	0.0262	0.0024	6.98		7.34	0.900	0.082	7.073
		14.150	0.0216	0.0034	7.36		7.76	0.764	0.120	7.131
		15.650	0.0121	0.0012	8.52		8.17	0.530	0.053	7.559
		16.425	0.0189	0.0031	7.63		8.38	1.024	0.168	7.986
		17.225	0.0169	0.0015	7.85		8.60	1.019	0.090	8.198
		18.350	0.0195	0.0025	7.57		8.91	1.305	0.167	8.407
		18.450	0.0118	0.0011	8.57		8.94	0.915	0.085	8.701
		19.475	0.0145	0.0018	8.16		9.22	1.139	0.141	8.727
		21.175	0.0088	0.0011	9.16		9.68	0.790	0.099	8.994
		21.910	0.0090	0.0008	9.11		9.88	1.009	0.090	9.438
		22.550	0.0107	0.0012	8.77		10.06	1.320	0.148	9.630
		23.675	0.0059	0.0006	9.96		10.37	0.791	0.080	9.797
ACEX (Arctic)	*Frank et al., 2008*	2.31	0.3849	0.0117	0.00		0.16	0.416	0.013	---
		4.64	0.8557	0.0257	-1.60	14.65	0.32	1.003	0.030	---
		8.71	0.3445	0.0105	0.22		0.59	0.464	0.014	---
		10.61	0.3135	0.0102	0.41		0.72	0.450	0.015	---
		14.31	0.4108	0.0150	-0.13		0.98	0.669	0.024	---
		16.19	0.3237	0.0105	0.35		1.11	0.563	0.018	---
		21.93	0.1664	0.0059	1.68		1.50	0.352	0.012	---
		24.86	0.2125	0.0064	1.19		1.70	0.496	0.015	---
		30.86	0.1333	0.0049	2.12		2.11	0.382	0.014	---
		35.62	0.0770	0.0028	3.22		2.43	0.260	0.009	---
		39.12	0.1052	0.0038	2.59		2.67	0.400	0.014	---
		43.76	0.0766	0.0037	3.23		2.99	0.341	0.016	---
		48.19	0.0635	0.0034	3.60		3.29	0.329	0.018	---
		52.84	0.0576	0.0024	3.80		3.61	0.350	0.015	---
		60.8	0.0504	0.0024	4.07		4.15	0.401	0.019	---
		65.3	0.0488	0.0023	4.13		4.46	0.453	0.021	---
		71.54	0.0411	0.0019	4.47		4.88	0.472	0.022	---
		75.08	0.0445	0.0022	4.31		5.13	0.577	0.029	---
		79.47	0.0708	0.0023	3.39		5.42	1.067	0.035	---
		86.9	0.0305	0.0017	5.07		5.93	0.592	0.033	---
		91.98	0.0288	0.0014	5.19		6.28	0.665	0.032	---
		102.03	0.0179	0.0010	6.14		6.96	0.582	0.033	---
		108.39	0.0148	0.0007	6.52		7.40	0.598	0.028	---
		112.9	0.0248	0.0012	5.48		7.71	1.169	0.057	---
		117.26	0.0081	0.0005	7.72		8.00	0.443	0.027	---
		122.4	0.0079	0.0006	7.77		8.36	0.515	0.039	---
		130.4	0.0062	0.0004	8.26		8.90	0.531	0.034	---
		135.49	0.0060	0.0004	8.32		9.25	0.612	0.041	---
						hiatus				
		140.44	0.0022	0.0004	10.33		11.59	0.722	0.131	---
		147.29	0.0022	0.0003	10.33		12.05	0.912	0.124	---
		151.28	0.0014	0.0003	11.23		12.33	0.665	0.143	---